Journal of Power Sources 248 (2014) 115–121

Contents lists available at ScienceDirect

Journal of Power Sources

journal homepage: www.elsevier.com/locate/jpowsour

Short communication

Ternary core/shell structure of Co_3O_4/NiO/C nanowire arrays as high-performance anode material for Li-ion battery

J.B. Wu*, R.Q. Guo*, X.H. Huang, Y. Lin

School of Physics & Electronic Engineering, Taizhou University, Taizhou, Zhejiang 318000, China

HIGHLIGHTS

- Construct a self-supported porous Co_3O_4/NiO/C core/shell nanowire array.
- Core/shell nanowire array shows high Li ion battery properties.
- Core/shell nanowire array structure is favorable for fast ion and electron transfer.

ARTICLE INFO

Article history:
Received 19 July 2013
Received in revised form
5 September 2013
Accepted 9 September 2013
Available online 19 September 2013

Keywords:
Core/shell
Cobalt oxide
Nickel oxide
Lithium ion battery
Nanowire

ABSTRACT

Self-supported core/shell nanowire arrays are highly desirable for designing high-performance electrochemical energy storage devices. Herein, we report self-supported ternary core/shell nanowire arrays of Co_3O_4/NiO/C on the nickel foam with the help of hydrothermal synthesis, chemical bath deposition and annealing carbonation methods. As an anode material for lithium ion batteries, the Co_3O_4/NiO/C core/shell nanowire arrays exhibit excellent electrochemical performances with lower polarization, higher capacity, improved cycle life and better high-rate capability than the pure Co_3O_4 nanowire arrays and single NiO nanoflake arrays. The enhanced electrochemical properties are mainly ascribed to the core/shell nanowire architecture with potential synergistic contribution such as improved mechanical stability and enhanced conductivity as well as faster ion/electron transfer.

1. Introduction

Lithium ion batteries (LIBs) are one of the most popular power sources for consumer electronics and electric vehicles [1–3]. To date, various materials have been exploited as the anode materials for LIBs, such as graphitic/non-graphitic carbon [4,5], graphene [6], transition metal oxides (Co_3O_4 [7], NiO [8], Fe_2O_3 [9], MnO_2 [10], SnO_2 [11], TiO_2 [12], WO_3 [13], etc.), Li alloys with Si and Sn [14,15], polymers [16], nitrides [17], and transition metal phosphide (M–P, M = Fe, Co, Ni, Cu, etc.) [17,18]. Among them, transition metal oxides have attracted extensive interest for LIBs due to their high theoretical capacity (several times larger than that of graphite, for example, the theoretical capacity of Co_3O_4 and NiO is 890 and 718 mA h g^{-1}, respectively), low cost, environmental friendliness, and natural abundance. However, they suffer from large volume expansion/contraction and severe aggregation associated with the Li^+ insertion and extraction process. These problems lead to electrode pulverization and loss of active materials, and cause a large irreversible capacity loss and poor cycling stability. Furthermore, the low conductivity of transition metal oxides aggravates the fading process especially at high current densities. It is highly desirable to design and fabricate high-performance transition metal oxides electrode by modifying or ameliorating their kinetics issue. To meet the requirement of high capacity and structural stability, one promising route is to scrupulously design nanoporous electrode materials and smart hybridization of bespoke materials [19–24].

Recently, a novel kind of electrode design, core/shell nanoarray structure, has been attracted great attention [20,21,25,26]. It has been proposed that integration of active materials into the core/shell hetero-structured nanoarrays can lead to further enhancement of the capacity and stability due to potential synergistic effects, for example, much more efficient utilization of the remaining free space, more efficient electrolyte penetration and structural stability [27,28]. This is especially important for the core/shell structures whose core and shell are both active metal oxides.

* Corresponding authors. Tel.: +86 576 88661937.
E-mail addresses: wujb@tzc.edu.cn (J.B. Wu), guorqtz@126.com (R.Q. Guo).

0378-7753/$ – see front matter © 2013 Elsevier B.V. All rights reserved.
http://dx.doi.org/10.1016/j.jpowsour.2013.09.040

Previously, Liu et al. [20] reported Co_3O_4 nanowire @MnO_2 ultrathin nanosheet core/shell arrays and their high-performance electrochemical properties as pseudo-capacitor electrode due to the unique core/shell structure and compositions. Besides, branched Co_3O_4/Fe_2O_3 nanowires reported by Zheng group showed higher specific capacity and cyclical stability than the single component as anode of LIBs [26]. Tu group synthesized hierarchical Fe_2O_3@Co_3O_4 nanowire array for LIBs and exhibited superior rate capability and cycling stability [29].

On the other hand, electrochemical performances of these core/shell nanomaterials are still unsatisfactory due to the lower conductivity of metal oxides compared with that of metal and carbon. A possible and facile method is to coat a thin layer of carbon on transition metal oxides to further improve the electrochemical performance. Previously, Tu group synthesized a nanosized $LiFePO_4$/C composite with a homogeneous and thin carbon-shell, and exhibited noticeable high rate capability and good cycling performance [30]. Recently, Chen et al. reported Co_3O_4 nanowire arrays coated by a thin layer of sputtered carbon and their improved electrochemical performances as compared to the bare Co_3O_4 [7]. The carbon shell not only provides a flexible buffer to accommodate the volume change during lithium insertion/extraction, but also increases the conductivity of the electrode. Even so, there is still much space for progress to fabricate high-performance Co_3O_4 based anode materials with enhanced cycle performance and high rate capability. Inspired by the results above, herein, we report a ternary Co_3O_4/NiO/C core/shell nanowire arrays synthesized via a three-step solution method with the aid of hydrothermal synthesis, chemical bath deposition and facile annealing carbonation. Free-standing Co_3O_4 nanowire arrays act as the backbone for the growth of NiO nanoflake shell and carbon layer. The electrochemical performances of the Co_3O_4/NiO/C core/shell nanowire arrays as the anode material for LIBs are fully characterized and show superior properties to the single Co_3O_4 nanowire and NiO nanoflake arrays.

2. Experimental

First, self-supported Co_3O_4 nanowire arrays were prepared by a facile hydrothermal synthesis method. The solution was prepared by dissolving 2 mmol of $Co(NO_3)_2$, 4 mmol NH_4F, and 10 mmol of $CO(NH_2)_2$ in 70 mL of distilled water. Then this resulting solution was transferred into Teflon-lined stainless steel autoclave linear. Nickel foams were immersed into the reaction solution. Top sides of the substrates were uniformly coated with a polytetrafluoroethylene tape to prevent the solution contamination. The linear was sealed in a stainless steel autoclave and maintained at 110 °C for 5 h and then cooled to room temperature. The samples were collected and rinsed with distilled water several times. Finally, the samples were annealed at 350 °C in normal purity argon for 2 h to obtain Co_3O_4 nanowire arrays. The porous Co_3O_4 nanowire arrays come from the thermal decomposition of precursor—basic cobalt carbonate hydroxide $Co_2(OH)_2CO_3$ nanowire arrays after heat-treatment. The reactions involved may be illustrated as follows [21].

$$Co^{2+} + xF^- \rightarrow [CoF_x]^{(x-2)-} \quad (1)$$

$$H_2NCONH_2 + H_2O \rightarrow 2NH_3 + CO_2 \quad (2)$$

$$CO_2 + H_2O \rightarrow CO_3^{2-} + 2H^+ \quad (3)$$

$$NH_3 \cdot H_2O \rightarrow NH_4^+ + OH^- \quad (4)$$

$$2[CoF_x]^{(x-2)-} + CO_3^{2-} + 2OH^- + nH_2O \rightarrow Co_2(OH)_2CO_3 \cdot nH_2O + 2xF^- \quad (5)$$

During annealing process:

$$3Co_2(OH)_2CO_3 \cdot nH_2O + O_2 \rightarrow 2Co_3O_4 + (3n+3)H_2O + 3CO_2 \quad (6)$$

Then, the self-supported Co_3O_4 nanowire arrays were used as the scaffold for the growth of NiO nanoflake shell in a simple chemical bath. The Co_3O_4 nanowire arrays grown on nickel foam (masked with polyimide tape to prevent deposition on the back sides) were placed vertically in a 250 mL Pyrex beaker. Solution for chemical bath deposition (CBD) was prepared by adding 20 mL of aqueous ammonia (25–28%) to the mixture of 100 mL of 1 M nickel sulfate and 80 mL of 0.25 M potassium persulfate. Immersing into the CBD solution for 8 min at 20 °C, the substrates were taken off and rinsed with distilled water. The samples were annealed at 350 °C in argon for 1.5 h. Then samples immersed into 0.05 M aqueous glucose solution for 12 h. Finally, the free-standing Co_3O_4/NiO/C core/shell nanowire arrays were formed by carbonization at 450 °C for 2 h in argon. The carbon comes from the decomposition of glucose. The precursor reactions for the growth of NiO nanoflake via CBD are represented as follows [31]:

$$[Ni(H_2O)_{6-x}(NH_3)_x]^{2+} + 2OH^- \rightarrow Ni(OH)_2 + (6-x)H_2O + xNH_3 \quad (7)$$

$$2Ni(OH)_2 + S_2O_8^{2-} + 2OH^- + H_2O \rightarrow 2NiOOH \cdot H_2O + 2SO_4^{2-} + 2H_2O \quad (8)$$

During annealing process:

$$NiOOH \cdot H_2O - e^- \rightarrow Ni(OH)_2 + OH^- \quad (9)$$

$$Ni(OH)_2 \rightarrow NiO + H_2O \quad (10)$$

For the sake of comparison, individual Co_3O_4 nanowire arrays and NiO nanoflake arrays were also prepared as the same preparation parameters on nickel foam substrates, respectively. The Co_3O_4 nanowire arrays were fabricated by the hydrothermal synthesis method in a 70 mL solution containing 2 mmol of $Co(NO_3)_2$, 4 mmol NH_4F, and 10 mmol of $CO(NH_2)_2$ and kept at 110 °C for 5 h. Then, the samples were annealed at 350 °C in normal purity argon for 2 h to obtain Co_3O_4 nanowire arrays. Meanwhile, the single NiO nanoflake arrays were prepared via the CBD method by adding 20 mL of aqueous ammonia (25–28%) to the mixture of 100 mL of 1 M nickel sulfate and 80 mL of 0.25 M potassium persulfate. Immersing into the CBD solution for 8 min at 20 °C, the nickel foam substrates were taken out and rinsed with distilled water. Finally, the samples were annealed at 350 °C in argon for 1.5 h to form NiO nanoflake arrays.

The morphologies and structures of the as-synthesized samples were characterized by field emission scanning electron microscopy (FESEM, FEI SIRION), X-ray diffraction (XRD, RIGAKU D/Max-2550 with Cu Kα radiation), transmission electron microscopy (TEM, JEOL JEM200CX), high-resolution transmission electron microscopy (HRTEM, JEOL JEM-2010F) and Raman spectroscopy (LABRAM HR-800).

For the electrochemical tests, CR2025 coin-type cells were directly fabricated from the core/shell nanowire arrays (Co_3O_4 mass ≈ 1.5 mg cm^{-2}, NiO mass ≈ 0.8 mg cm^{-2}, C

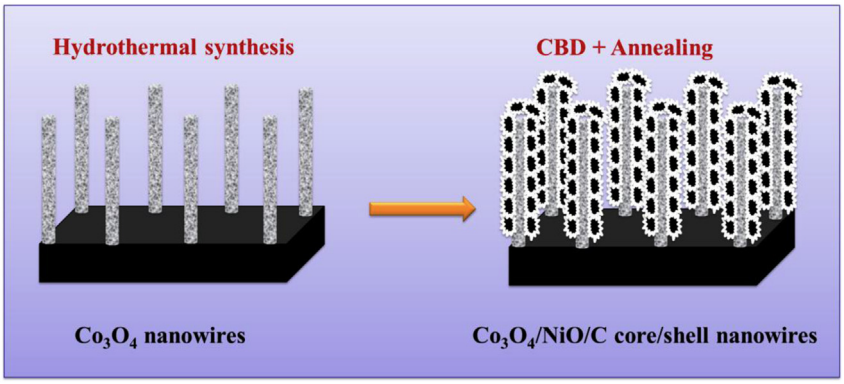

Fig. 1. Schematic diagram for the fabrication process of Co_3O_4/NiO/C.

mass ≈ 0.1 mg cm^{-2}) on nickel foam as the working electrode without any ancillary materials. For the single Co_3O_4 nanowire arrays, the mass of Co_3O_4 is ≈ 1.5 mg cm^{-2}. For the single NiO nanoflake arrays, the mass of NiO is ≈ 0.8 mg cm^{-2}. A metallic lithium foil served as the counter electrode, 1 M $LiPF_6$ in ethylene carbonate (EC)–dimethyl carbonate (DMC) (1:1 in volume) was used as the electrolyte, and a polypropylene micro-porous film (Cellgard 2300) was used as the separator. The cells were assembled in an argon-filled glove box with high-purity argon gas. The galvanostatic charge/discharge tests were performed on a LAND battery program-control test system (Wuhan, China) between 0 and 3.2 V at room temperature. The cyclic voltammetry (CV) test was carried out on a CHI660C electrochemical workstation (Chenhua, Shanghai) in the potential window of 0–3 V (vs. Li/Li^+) at a scan rate of 0.1 mV s^{-1}.

3. Results and discussion

Fig. 1 illustrates schematically the formation process of Co_3O_4/NiO/C nanowire array on Ni foam. The hydrothermally synthesized Co_3O_4 nanowire arrays serves as the backbone for the following deposition of NiO nanoflakes and carbon. Fig. 2 shows the XRD patterns of NiO nanoflakes, Co_3O_4 nanowire, and Co_3O_4/NiO/C core/shell nanowire arrays. In order to reduce the strong impact of the Ni foam substrate on the XRD peak signals, all samples are scratched from Ni foam for XRD analysis. As shown in Fig. 2, the XRD confirms that the core/shell nanowire arrays contain spinel Co_3O_4 phase (JCPDS 42-1467) [28], and cubic NiO phase (JCPDS 4-0835) [32]. No obvious carbon diffraction peaks are observed, indicating that the carbon deposited by decomposing the glucose is amorphous.

Fig. 3 shows the morphologies of the Co_3O_4 nanowires grown on Ni foam. Obviously, the nickel foam is uniformly covered by the Co_3O_4 nanowires with sharp tips and average diameter of 90 nm, which is also confirmed by TEM in Fig. 3c. Further insight into the detailed microstructure of the core/shell nanowire is demonstrated by TEM and HRTEM. As shown in the TEM images of the Co_3O_4 nanowires (Fig. 3c and d), these needle-like nanowires are highly porous and composed of nanoparticles of ~4 nm. The measured lattice spacing is 0.46 nm which is in good agreement with the (111) interplanar distance of the spinel Co_3O_4 phase (JCPDS 42-1467) [33].

The morphologies of single NiO nanoflakes film grown on Ni foam substrate are shown in Fig. 4. The NiO thin film exhibits a highly porous net-like structure made up of many interconnected nanoflakes with thicknesses of ~15 nm. The NiO nanoflakes are thin and flat with low level roughness. The nanoflakes arrange vertically to the substrate, forming a net-like structure and leaving pores of 30–300 nm (Fig. 4a and b). In addition, all the diffraction rings in the SAED pattern of the nanoflake can be indexed with the cubic NiO phase (JPCDS 4-0835), indicating that the porous NiO film is polycrystalline in nature, which is also confirmed by the XRD in Fig. 2a.

After loading of the NiO nanoflakes by CBD and carbon by carbonization, Co_3O_4 nanowires are decorated by interconnected NiO/C nanoflakes shell forming ternary Co_3O_4/NiO/C core/shell nanowires with diameter of ~230 nm. The hybrid nanoflake shell is vertically arranged to the Co_3O_4 core (Fig. 5a, b). Obviously, no NiO particles are packed in the interspace among the nanowires, suggesting that the NiO nanoflakes are preferentially grown on the Co_3O_4 surface. Importantly, Co_3O_4/NiO/C core/shell nanowires still retain the uniform array structure. From the TEM (Fig. 5c and d), it is observed that the Co_3O_4 nanowire core is tightly bonded and covered by ultrathin NiO/C nanoflakes, forming typical core/shell hetero-structured architecture. The high resolution TEM (HRTEM) image shown in Fig. 5e reveals a distinct set of visible lattice fringes with an inter-planar spacing of 0.27 nm, corresponding to the (100) plane of cubic NiO phase (JCPDS 4-0835). In addition, the SAED pattern of NiO/C shell shows no difference from that of NiO nanoflakes in Fig. 4c, indicating that the carbon is amorphous. The HTEM in Fig. 5e shows that the carbon shell is ~3 nm thick and its amorphous nature. This composition is clearly distinguished by energy dispersive X-ray spectroscopic (EDS) elemental maps of Co, Ni, O and C from the designated area in Fig. 5d. In addition, the EDS spectrum verifies the composition of the core/shell nanowire to be Co, Ni, O and C (Fig. 6a), which is in agreement with the EDS mapping result above. The layer of amorphous carbon is also

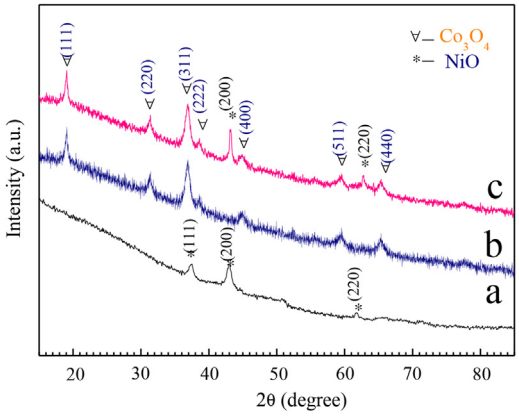

Fig. 2. XRD patterns of films scratched from substrates: (a) NiO, (b) Co_3O_4, (c) Co_3O_4/NiO/C.

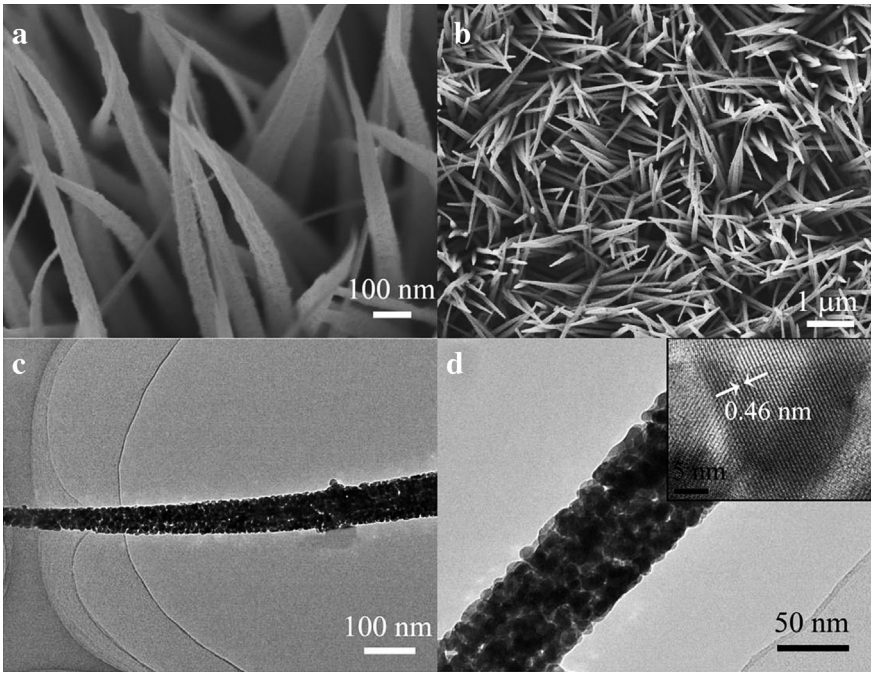

Fig. 3. The morphology of Co_3O_4 nanowire arrays: (a) and (b) SEM in different magnification. (c) and (d) TEM and HRTEM.

confirmed by Raman spectrum (Fig. 6b), which clearly shows two obvious peaks located at 1344 cm^{-1} (D-band) and 1593 cm^{-1} (G-band), which are characteristic of amorphous carbon [34].

The electrochemical performances of these nanowire arrays as anode materials for LIBs are investigated and shown in Fig. 7. Fig. 7a shows the CV tests of Co_3O_4, NiO and Co_3O_4/NiO/C electrodes separately in the potential range of 0–3 V in the second cycle. For the Co_3O_4/NiO/C electrode, a low-intensity peak is found near 1.3 V, which refers to the formation of a partially reversible SEI layer. Two cathodic peaks are observed at about 0.85 V and 0.97 V, corresponding to the reduction of NiO and Co_3O_4 to Ni and Co nanoparticles, respectively. Anodic peaks at around 1.53 V and 2.19 V correspond to the partial decomposition of SEI layer and the decomposition of Li_2O and nanometal particles (Ni, Co) converted back to metal oxides, respectively [3]. In addition, the integral area of Co_3O_4/NiO/C electrode is larger than those of the pristine NiO and Co_3O_4, indicating that more reactions toward Li^+ occur in the Co_3O_4/NiO/C electrode. Moreover, the Co_3O_4/NiO/C electrode

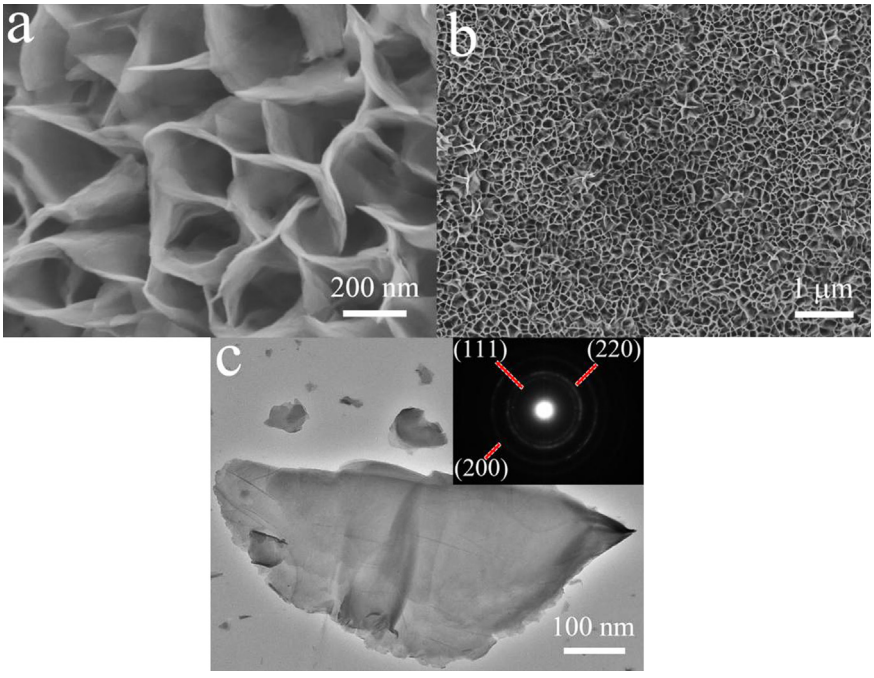

Fig. 4. The morphology of NiO nanoflake arrays: (a) and (b) SEM in different magnification. (c) TEM (inset: SAED pattern).

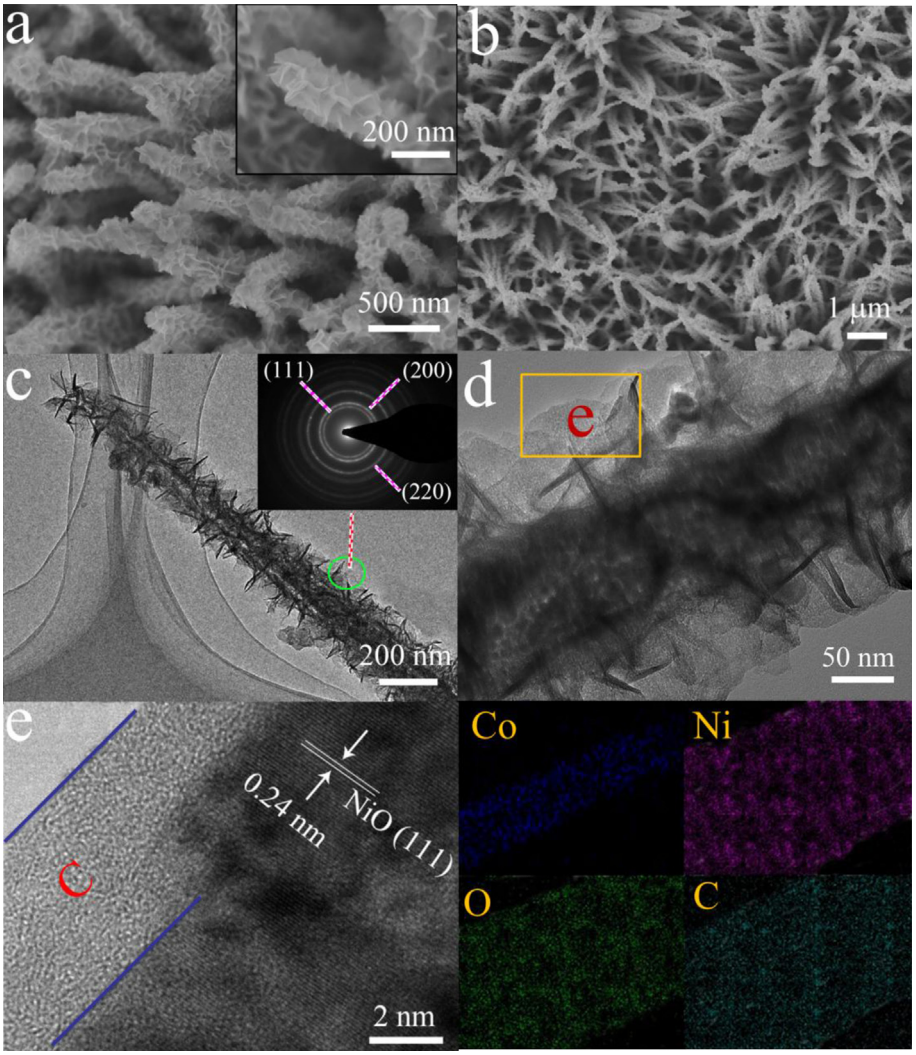

Fig. 5. The morphology of Co_3O_4/NiO/C nanowire arrays: (a) and (b) SEM in different magnification. (c) and (d) TEM images (inset: SAED pattern). (e) HRTEM. (f) EDS mapping of Co, Ni, C and O.

exhibits higher current densities than that of each single component and Co_3O_4/NiO nanowire arrays, indicating its higher electrochemical activity during cycling.

Fig. 7b shows the cycling performance of the three electrodes between 0.01 V and 3 V at 0.5 C. The Co_3O_4/NiO/C electrode delivers an initial discharge capacity of 1426 mA h g^{-1} and a good capacity retention. After 50 cycles, it still retains a capacity of 1053 mA h g^{-1}. While the Co_3O_4 nanowire electrode shows an initial discharge capacity of 1221 mA h g^{-1} and retains only 724 mA h g^{-1} after 50 cycles and the capacity retention of 59% is lower than that of the

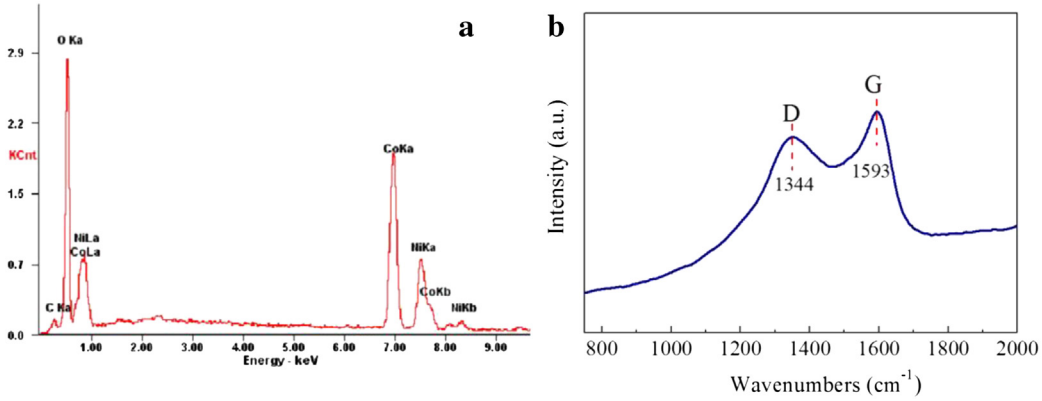

Fig. 6. (a) Raman spectrum, (b) EDX spectrum of Co_3O_4/NiO/C nanowire array film.

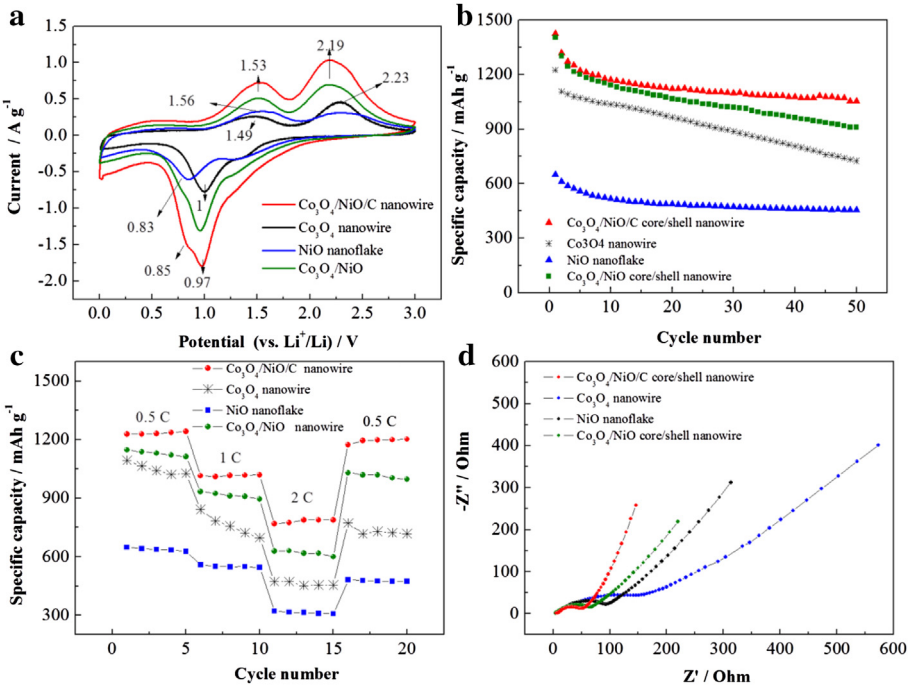

Fig. 7. Electrochemical characterizations of four array electrodes: (a) CV curves at a scan rate of 0.1 mV s^{-1} between 0 and 3.0 V at the second cycle, (b) cycling performances at 0.5 C. (c) Rate capability. (d) Nyquist plots of three array electrodes at discharge state at 5th cycle.

Co_3O_4/NiO/C electrode, which is 73.8%. For the single NiO nanoflakes, it only shows a specific capacity of 649 mA h g^{-1} at first cycle and 69% capacity retention after 50 cycles, lower than those of Co_3O_4/NiO/C electrode. For the Co_3O_4/NiO nanowire arrays without carbon layer, they show better cycling stability (897 mA h g^{-1} after 50 cycles) than the single components, but inferior to the Co_3O_4/NiO/C nanowire arrays. The rate capability of the core/shell nanowire array at progressively increased current density is recorded in Fig. 7c. The discharge capacities of the Co_3O_4/NiO/C nanowire arrays at rates of 0.5, 1, 2 C and 0.5 C are 1227, 1014, 769 and 1174 mA h g^{-1}, respectively, which are much higher than those of Co_3O_4/NiO nanowire arrays (1109, 893, 600 and 1004 mA h g^{-1}), pristine Co_3O_4 (1093, 842, 477 and 772 mA h g^{-1}) and NiO (648, 559, 321 and 481 mA h g^{-1}). The capacity of Co_3O_4/NiO/C electrode has only a little fading when the discharge rate returns from 2 C to 0.5 C. This enhancement of performance is further confirmed by the electrochemical impedance spectroscopy (EIS) measurements (Fig. 7d), which were carried out at 5th cycle at 0.5 C. Nyquist plots

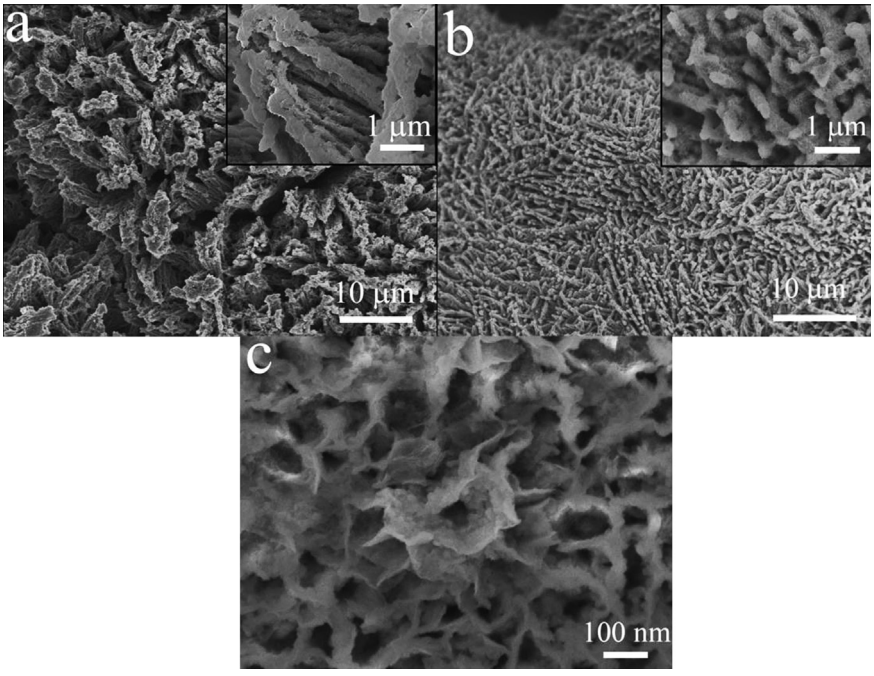

Fig. 8. SEM images of (a) Co_3O_4, (b) Co_3O_4/NiO/C and (c) NiO electrodes after 15 cycles at 0.5 C.

consist of depressed semicircle in the high-frequency region and a long low-frequency line. Apparently, the semicircle diameter of the Co_3O_4/NiO/C electrode is smaller than that of Co_3O_4/NiO nanowire arrays and the single component, indicating the Co_3O_4/NiO/C electrode possesses a good electronic wetting and thus a rapid charge transfer reaction during the lithium uptake and extraction, resulting in higher reactivity and faster reaction kinetics. It is indicated that the introduction is especially helpful for the enhancement of high-rate capability and fast reaction kinetics.

It is believed that the synergistic contribution from ultrathin NiO nanoflakes, the porous Co_3O_4 nanowires, the layer of amorphous carbon, and the ordered porous nanowire array should account for the good cycle performance and rate capability. First, the core/shell nanowire arrays grow directly on conductive substrates to form integrated electrode, which is regarded as beneficial to improve the electric connection between the active material and current collector, and reducing the "dead volume" and resistance possibly caused by the polymer binder. Second, the high porosity and large surface area rendered by the nanowire core and nanoflake branches enhance the electrolyte–material contact area and provide short ion/electron diffusion path, which is very critical to high-power energy storage. Third, the introduction of carbon can effectively improve the electric conductivity of the electrode to ensure fast electron transfer at high-rates. Another key advantage of this core/shell architecture is robust mechanical stability, which can accommodate structural strains and favor an enhanced calendar life. After 15 cycles at 0.5 C, we disassembled the batteries and observed morphologies of electrodes using FESEM. The morphology of the Co_3O_4/NiO/C array remains much more integrated after the lithiation–delithiation cycles (Fig. 8b), compared to that of Co_3O_4 (Fig. 8a) and NiO (Fig. 8c), which start to pulverize and the whole structure disintegrate, indicating that the core/shell structure and introduction of carbon layer are beneficial to relax the volume expansion and alleviates the structure damage of the nanowires during cycling.

4. Conclusions

A core/shell Co_3O_4/NiO/C nanowire array is successfully synthesized via a three-step solution method. In this core/shell structure, the porous Co_3O_4 core acts as the backbone for the growth of ultrathin NiO nanoflakes. A layer of amorphous carbon is evenly deposited on the surface of active metal oxides. The reversible specific capacity after 50 cycles for the core/shell array is 1053 mA h g^{-1} at 0.5 C, which is higher than that of the pure Co_3O_4 nanowire array film (724 mA h g^{-1}) and NiO nanoflake film (454 mA h g^{-1}). The excellent electrochemical performance can be ascribed to the synergetic contribution from the porous Co_3O_4 nanowire core and the ultrathin NiO nanoflake shell, as well as the ordered array geometry and the introduction of carbon layer.

Acknowledgment

The authors would like to acknowledge financial support from Zhejiang Provincial Natural Science Foundation of China (Grant No. Y4110628) and National Natural Science Foundation of China (Grant No. 51204116).

References

[1] M. Armand, J.M. Tarascon, Nature 451 (2008) 652.
[2] K.S. Kang, Y.S. Meng, J. Breger, C.P. Grey, G. Ceder, Science 311 (2006) 977.
[3] P. Poizot, S. Laruelle, S. Grugeon, L. Dupont, J.M. Tarascon, Nature 407 (2000) 496.
[4] N.A. Kaskhedikar, J. Maier, Adv. Mater. 21 (2009) 2664.
[5] B.J. Landi, M.J. Ganter, C.D. Cress, R.A. DiLeo, R.P. Raffaelle, Energy Environ. Sci. 2 (2009) 638.
[6] Z.L. Wang, D. Xu, Y. Huang, Z. Wu, L.M. Wang, X.B. Zhang, Chem. Commun. 48 (2012) 976.
[7] J. Chen, X.H. Xia, J.P. Tu, Q.Q. Xiong, Y.X. Yu, X.L. Wang, C.D. Gu, J. Mater. Chem. 22 (2012) 15056.
[8] Y.J. Mai, J.P. Tu, X.H. Xia, C.D. Gu, X.L. Wang, J. Power Sources 196 (2011) 6388.
[9] J. Chen, L.N. Xu, W.Y. Li, X.L. Gou, Adv. Mater. 17 (2005) 582.
[10] H.G. Wang, Z.G. Lu, D. Qian, Y.J. Li, W. Zhang, Nanotechnology 18 (2007).
[11] H. Kim, J. Cho, J. Mater. Chem. 18 (2008) 771.
[12] D.H. Wang, D.W. Choi, J. Li, Z.G. Yang, Z.M. Nie, R. Kou, D.H. Hu, C.M. Wang, L.V. Saraf, J.G. Zhang, I.A. Aksay, J. Liu, ACS Nano 3 (2009) 907.
[13] K. Huang, Q. Pan, F. Yang, S. Ni, X. Wei, D. He, J. Phys. D Appl. Phys. 41 (2008).
[14] J.P. Rong, C. Masarapu, J. Ni, Z.J. Zhang, B.Q. Wei, ACS Nano 4 (2010) 4683.
[15] C.D. Gu, Y.J. Mai, J.P. Zhou, Y.H. You, J.P. Tu, J. Power Sources 214 (2012) 200.
[16] P. Novak, K. Muller, K.S.V. Santhanam, O. Haas, Chem. Rev. 97 (1997) 207.
[17] J.L.C. Rowsell, V. Pralong, L.F. Nazar, J. Am. Chem. Soc. 123 (2001) 8598.
[18] Y. Lu, J.P. Tu, C.D. Gu, X.L. Wang, S.X. Mao, J. Mater. Chem. 21 (2011) 17988.
[19] Y.Y. Liang, Y.G. Li, H.L. Wang, J.G. Zhou, J. Wang, T. Regier, H.J. Dai, Nat. Mater. 10 (2011) 780.
[20] J.P. Liu, J. Jiang, C.W. Cheng, H.X. Li, J.X. Zhang, H. Gong, H.J. Fan, Adv. Mater. 23 (2011) 2076.
[21] X.H. Xia, J.P. Tu, Y.Q. Zhang, X.L. Wang, C.D. Gu, X.B. Zhao, H.J. Fan, ACS Nano 6 (2012) 5531.
[22] J. Zhong, X.L. Wang, X.H. Xia, C.D. Gu, J.Y. Xiang, J. Zhang, J.P. Tu, J. Alloys Compd. 509 (2011) 3889.
[23] W.W. Zhou, J.P. Liu, T. Chen, K.S. Tan, X.T. Jia, Z.Q. Luo, C.X. Cong, H.P. Yang, C.M. Li, T. Yu, Phys. Chem. Chem. Phys. 13 (2011) 14462.
[24] Z.S. Wu, W.C. Ren, L. Wen, L.B. Gao, J.P. Zhao, Z.P. Chen, G.M. Zhou, F. Li, H.M. Cheng, ACS Nano 4 (2010) 3187.
[25] Y.J. Chen, F. Zhang, G.G. Zhao, X.Y. Fang, H.B. Jin, P. Gao, C.L. Zhu, M.S. Cao, G. Xiao, J. Phys. Chem. C 114 (2010) 9239.
[26] H. Wu, M. Xu, Y.C. Wang, G.F. Zheng, Nano Res. 6 (2013) 167.
[27] X.H. Xia, J.S. Luo, Z.Y. Zeng, C. Guan, Y.Q. Zhang, J.P. Tu, H. Zhang, H.J. Fan, Sci. Rep. 2 (2012).
[28] X.H. Xia, J.P. Tu, Y.Q. Zhang, J. Chen, X.L. Wang, C.D. Gu, C. Guan, J.S. Luo, H.J. Fan, Chem. Mater. 24 (2012) 3793.
[29] Q.Q. Xiong, X.H. Xia, J.P. Tu, J. Chen, Y.Q. Zhang, D. Zhou, C.D. Gu, X.L. Wang, J. Power Sources 240 (2013) 344.
[30] W.L. Liu, J.P. Tu, Y.Q. Qiao, J.P. Zhou, S.J. Shi, X.L. Wang, C.D. Gu, J. Power Sources 196 (2011) 7728.
[31] X.H. Xia, J.P. Tu, X.L. Wang, C.D. Gu, X.B. Zhao, J. Mater. Chem. 21 (2011) 671.
[32] X.H. Xia, J.P. Tu, Y.J. Mai, R. Chen, X.L. Wang, C.D. Gu, X.B. Zhao, Chem. Eur. J. 17 (2011) 10898.
[33] X.H. Xia, J.P. Tu, Y.Q. Zhang, Y.J. Mai, X.L. Wang, C.D. Gu, X.B. Zhao, RSC Adv. 2 (2012) 1835.
[34] J.P. Liu, Y.Y. Li, R.M. Ding, J. Jiang, Y.Y. Hu, X.X. Ji, Q.B. Chi, Z.H. Zhu, X.T. Huang, J. Phys. Chem. C 113 (2009) 5336.